

# Update analysis of $\tau^- \rightarrow VP^- \nu_\tau$ : Theory and Experiment

Zhi-Hui Guo <sup>a b \*</sup>

<sup>a</sup> Department of Physics, Peking University, Beijing 100871, P. R. China,

<sup>b</sup> IFIC, CSIC-Universitat de València, Apt. Correus 22085, E-46071, València, Spain

Within the resonance chiral theory (R $\chi$ T), we have studied the process of a tau lepton decaying into a vector resonance plus a pseudo-Goldstone meson and a tau neutrino. Two kinds of processes are discussed: (a)  $\tau^- \rightarrow (\rho^0 \pi^-, \omega \pi^-, \phi \pi^-, K^{*0} K^-) \nu_\tau$ , belonging to  $\Delta S = 0$  processes and (b)  $\Delta S = 1$  processes, such as  $\tau^- \rightarrow (\rho^0 K^-, \omega K^-, \phi K^-, \bar{K}^{*0} \pi^-) \nu_\tau$ . To fit the  $\tau^- \rightarrow \omega \pi^- \nu_\tau$  spectral function and the decay distribution of  $\tau^- \rightarrow \omega K^- \nu_\tau$  to get unknown resonance couplings, we then make a prediction for branching ratios of all channels.

## 1. Introduction

Due to its clean background,  $\tau$  decay can provide an excellent environment to study the non-perturbative dynamics of QCD. In these decays, the intermediate resonances may play an important role. Moreover, due to the improvement of statistically significant measurements, the branching ratios and spectral functions of the processes containing resonances in the final states of  $\tau$  decays have also been determined in recent experiments [1][2][3][4][5]. Motivated by the new measurements, we perform the study of tau decaying into a resonance plus a pseudo-Goldstone meson and a tau neutrino in this work.

Combining the  $SU(3)_L \times SU(3)_R$  chiral symmetry, that drives the interaction of pseudo-Goldstone mesons resulting from the spontaneous chiral symmetry breaking of QCD and the  $SU(3)_V$  symmetry for the resonance multiplets, the resonance chiral lagrangians consisting of specific number of resonance multiplets have been written down in [6][7]. To build a more realistic QCD-like effective theory, large- $N_C$  techniques and short-distance constraints from QCD

\*I would like to thank the organizers of QCD 2008 for providing the charming atmosphere in the conference and also the nice social events. ZHG is supported in part by China Scholarship Council and National Nature Science Foundation of China under grant number 10721063 and 10575002. This work is also partially supported by EU Contract No. MRTN-CT-2006-035482 (FLAVIANet), by MEC (Spain) under grant FPA2007-60323 and by Spanish Consolider-Ingénio 2010 Programme CPAN (CSD2007-00042).

have been implemented into the resonance effective theory to constraint resonance couplings [8][9][10][11]. Therefore, resonance chiral effective theory can be a perfect tool to study hadronic  $\tau$  decays. Indeed it has already been employed in the studies of  $\tau \rightarrow \pi K \nu_\tau$  [12],  $\tau \rightarrow \pi \pi \nu_\tau$  [13] and  $\tau \rightarrow K \bar{K} \nu_\tau$  [14].

In Ref.[15], we have made a comprehensive analysis for tau decaying into a vector resonance plus a pseudo-Goldstone meson and a tau neutrino: (a)  $\Delta S = 0$  processes, such as  $\tau^- \rightarrow (\rho^0 \pi^-, \omega \pi^-, \phi \pi^-, K^{*0} K^-) \nu_\tau$  and (b)  $\Delta S = 1$  processes, like  $\tau^- \rightarrow (\rho^0 K^-, \omega K^-, \phi K^-, \bar{K}^{*0} \pi^-) \nu_\tau$ , in the frame of R $\chi$ T. The main results will be presented in this paper.

## 2. Theoretical frame for tau decays

The amplitude for  $\tau^-(p) \rightarrow P^-(p_1) V(p_2) \nu_\tau(q)$ , where  $P^-$  can be  $\pi^-, K^-$  and  $V$  can be  $\rho^0, \omega, \phi, K^{*0}, \bar{K}^{*0}$ , has the general structure

$$\begin{aligned} & -G_F V_{uQ} \bar{u}_{\nu_\tau}(q) \gamma^\mu (1 - \gamma_5) u_\tau(p) \\ & \times \epsilon_V^{*\nu}(p_2) \left[ v \varepsilon_{\mu\nu\rho\sigma} p_1^\rho p_2^\sigma \right. \\ & \left. - (a_1 g_{\mu\nu} + a_2 p_{1\mu} p_{1\nu} + a_3 p_{2\mu} p_{1\nu}) \right], \end{aligned} \quad (1)$$

where  $G_F$  is the Fermi constant;  $V_{uQ}$  is the CKM matrix element;  $\varepsilon_{\mu\nu\rho\sigma}$  is the anti-symmetric Levi-Civita tensor;  $\epsilon_V^{*\mu}(p_2)$  is the polarization vector for the vector resonance;  $v$  denotes the form factor of the vector current and  $a_1, a_2, a_3$  are the corresponding axial-vector form factors.

The form factors in Eq.(1) will be calculated within R $\chi$ T. The relevant R $\chi$ T lagrangian that we will use in this paper is

$$\begin{aligned} \mathcal{L}_{R\chi T} = & \frac{F^2}{4} \langle u_\mu u^\mu + \chi_+ \rangle + \mathcal{L}^{kin}(V, A) + \mathcal{L}_{2V,A} \\ & + \mathcal{L}_{VVP} + \mathcal{L}_{VJP} + \mathcal{L}_{VAP} + \mathcal{L}_{VV_1P}, \end{aligned} \quad (2)$$

where the first term is the leading order operators of the chiral perturbation theory [16]; the antisymmetric tensor formalism will be used to describe the vector and axial-vector resonances; the kinematics terms  $\mathcal{L}^{kin}(V, A)$  and the operators only containing one multiplet of resonances  $\mathcal{L}_{2V,A}$  can be found in [6]; the operators containing two resonance multiplets:  $\mathcal{L}_{VVP}, \mathcal{L}_{VJP}, \mathcal{L}_{VAP}$ , can be found in [10][11]; the interaction terms between the lowest vector multiplet  $V$  and the heavier multiplet  $V_1$  can be found in [17]. The SU(3) matrices for vector and axial-vector resonances are given by

$$V = \begin{pmatrix} \frac{\rho_0}{\sqrt{2}} + \frac{\omega_8}{\sqrt{6}} + \frac{\omega_1}{\sqrt{3}} & \rho^+ & K^{*+} \\ \rho^- & -\frac{\rho_0}{\sqrt{2}} + \frac{\omega_8}{\sqrt{6}} + \frac{\omega_1}{\sqrt{3}} & K^{*0} \\ K^{*-} & -\frac{2\omega_8}{\sqrt{6}} + \frac{\omega_1}{\sqrt{3}} & \end{pmatrix},$$

$$A = \begin{pmatrix} \frac{a_1^0}{\sqrt{2}} + \frac{f_1^8}{\sqrt{6}} + \frac{f_1^1}{\sqrt{3}} & a_1^+ & K_{1A}^+ \\ a_1^- & -\frac{a_1^0}{\sqrt{2}} + \frac{f_1^8}{\sqrt{6}} + \frac{f_1^1}{\sqrt{3}} & K_{1A}^0 \\ K_{1A}^- & -\frac{2f_1^8}{\sqrt{6}} + \frac{f_1^1}{\sqrt{3}} & \end{pmatrix},$$

and  $K_{1A}$  is related to the physical states  $K_1(1270), K_1(1400)$  through:

$$K_{1A} = \cos\theta K_1(1400) + \sin\theta K_1(1270). \quad (3)$$

About the discussion on the nature of  $K_1(1270)$  and  $K_1(1400)$ , one can see [18] for details. For the vector resonances  $\omega$  and  $\phi$ , we assume the ideal mixing for them throughout:

$$\omega_1 = \sqrt{\frac{2}{3}}\omega - \sqrt{\frac{1}{3}}\phi, \quad \omega_8 = \sqrt{\frac{2}{3}}\phi + \sqrt{\frac{1}{3}}\omega. \quad (4)$$

The corresponding Feynman diagrams contributed to the form factors  $v, a_1, a_2, a_3$  in the process of  $\tau^-(p) \rightarrow K^-(p_1)\rho^0(p_2)\nu_\tau(q)$  are given in Fig.(1) and Fig.(2).

The explicit expressions for the form factors  $v, a_1, a_2, a_3$  of  $\tau^-(p) \rightarrow K^-(p_1)\rho^0(p_2)\nu_\tau(q)$  can be found in [15]. The corresponding form factors of other channels are quite similar to the ones of

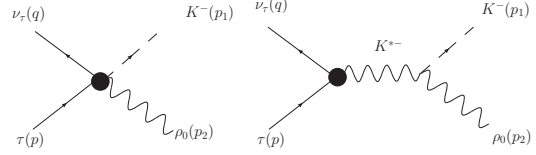


Figure 1. Diagrams appearing in the vector current of  $\tau^-(p) \rightarrow K^-(p_1)\rho^0(p_2)\nu_\tau(q)$ .

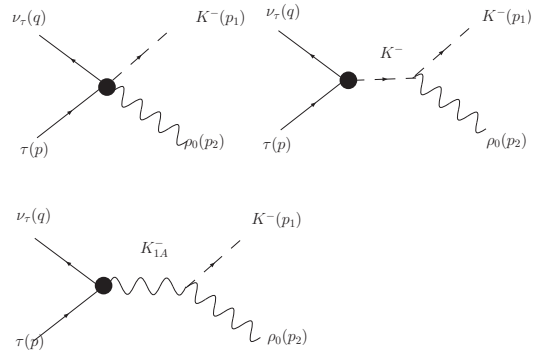


Figure 2. Diagrams appearing in the axial-vector current of  $\tau^-(p) \rightarrow K^-(p_1)\rho^0(p_2)\nu_\tau(q)$ .

$\tau^-(p) \rightarrow K^-(p_1)\rho^0(p_2)\nu_\tau(q)$  and one can find the explicit expressions in the Appendix of [15].

Since most of the intermediate resonances have wide decay widths, the off-shell widths of these resonances may play an important role in the dynamics of  $\tau$  decays. To introduce the finite decay widths for the resonances implies that the corrections from the next-to-leading order of  $1/N_C$  expansion are taken account into our game. This issue has been discussed in [19] for the decay width of  $\rho(770)$  and we take the result of that article

$$\Gamma_\rho(s) = \frac{sM_V}{96\pi F^2} \left[ \sigma_\pi^3 \theta(s - 4m_\pi^2) + \frac{1}{2} \sigma_K^3 \theta(s - 4m_K^2) \right],$$

where  $\sigma_P = \sqrt{1 - 4m_P^2/s}$  and  $\theta(s)$  is the step function. About the energy dependent widths for  $\rho', K^*, K^{*'}, K_1(1270), K_1(1400), a_1(1260)$ , we follow the way introduced in [12] to construct them

	Exp.	One multiplet	Fit 1	Fit 2
$B(\tau^- \rightarrow \rho^0 \pi^- \nu_\tau)$	—	$8.1 \times 10^{-2}$	$9.4 \times 10^{-2}$	$8.1 \times 10^{-2}$
$B(\tau^- \rightarrow \omega \pi^- \nu_\tau)$	$(1.95 \pm 0.08) \times 10^{-2}$	$0.17 \times 10^{-2}$	$2.1 \times 10^{-2}$	$2.1 \times 10^{-2}$
$B(\tau^- \rightarrow K^{*0} K^- \nu_\tau)$	$(2.1 \pm 0.4) \times 10^{-3}$	$1.4 \times 10^{-3}$	$1.5 \times 10^{-3}$	$1.5 \times 10^{-3}$

Table 1

Branching ratios for  $\Delta S = 0$  processes. The second column denotes experimental values, which are taken from [1]. The values from the third column to the fifth column denote our predictions under different assumptions: only including the lowest multiplet, the fitting results with  $\lambda' = 0.455$ ,  $\lambda'' = -0.0938$ ,  $\lambda_0 = 0.0904$  (Fit 1) and the fitting results with  $\lambda' = 0.5$ ,  $\lambda'' = 0$ ,  $\lambda_0 = 0.125$  (Fit 2). It is interesting to notice that a recently reported number:  $B(\tau^- \rightarrow K^{*0} K^- \nu_\tau) = (1.56 \pm 0.02 \pm 0.09) \times 10^{-3}$  [20], is highly consistent with our predictions.

	Exp	One multiplet	Fit 1	Fit 2
$B(\tau^- \rightarrow \rho^0 K^- \nu_\tau)$	$(1.6 \pm 0.6) \times 10^{-3}$	$3.9 \times 10^{-4}$	$4.7 \times 10^{-4}$	$3.5 \times 10^{-4}$
$B(\tau^- \rightarrow \omega K^- \nu_\tau)$	$(4.1 \pm 0.9) \times 10^{-4}$	$3.5 \times 10^{-4}$	$4.0 \times 10^{-4}$	$3.0 \times 10^{-4}$
$B(\tau^- \rightarrow \phi K^- \nu_\tau)$	$(4.05 \pm 0.36) \times 10^{-5}$ (Belle) $(3.39 \pm 0.34) \times 10^{-5}$ (BABAR)	$1.7 \times 10^{-5}$	$1.8 \times 10^{-5}$	$1.6 \times 10^{-5}$
$B(\tau^- \rightarrow \bar{K}^{*0} \pi^- \nu_\tau)$	$(2.2 \pm 0.5) \times 10^{-3}$	$3.3 \times 10^{-3}$	$5.1 \times 10^{-3}$	$4.0 \times 10^{-3}$

Table 2

Branching ratios for  $\Delta S = 1$  processes. The meaning of numbers in different columns is the same to Table 1. The experimental values for  $\phi K^-$  are taken from [4] and [5]. The remaining experimental data is taken from [1].

and the explicit formulae can be found in [15].

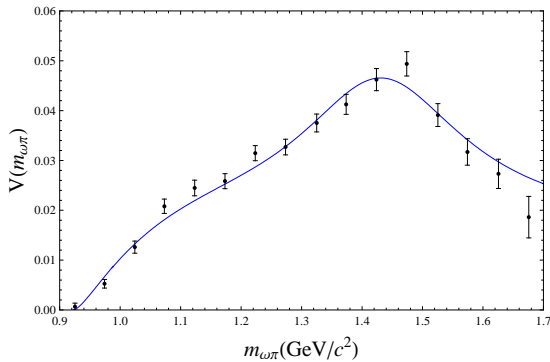


Figure 3. Spectral function for  $\tau^- \rightarrow \omega \pi^- \nu_\tau$ . The experimental data are taken from [2].

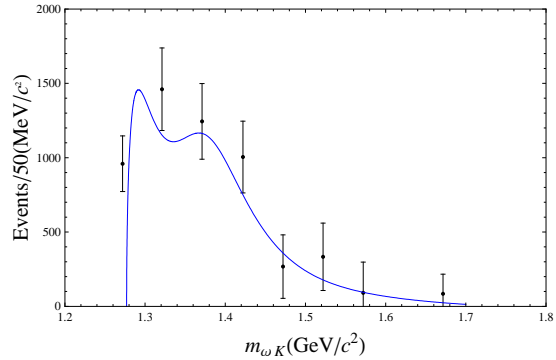


Figure 4. Invariant mass distribution for  $\omega K^-$  in the process  $\tau^- \rightarrow \omega K^- \nu_\tau$ . The experimental data are taken from [3].

### 3. Phenomenological discussion

Although some related resonance couplings can be fixed by imposing QCD short distance constraints [10][11][15], we still have 5 free parameters:  $d_3$ , a resonance coupling related to the low-

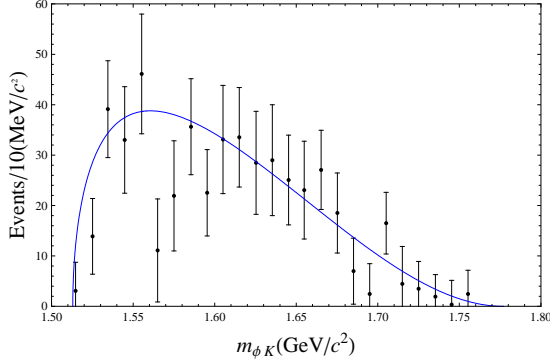


Figure 5. Predicted invariant mass distribution for  $\phi K^-$  in the process  $\tau^- \rightarrow \phi K^- \nu_\tau$ . The experimental data are taken from [4], where only the data up to  $m_{\phi K} = 1.75$  GeV are quoted in the plot.

est vector multiplet;  $d_m, d_M, d_s$ , the couplings for the excited vector multiplet  $V_1$ ; the mixing angle  $\theta$ , a parameter for the axial-vector resonances defined in Eq.(3). We fit the 5 parameters using the  $\tau^- \rightarrow \omega \pi^- \nu_\tau$  spectral function and the invariant mass distribution of  $\omega K$  system in the process of  $\tau^- \rightarrow \omega K^- \nu_\tau$ . To test the stability, we take two sets of values for the axial- vector resonance couplings  $\lambda_i$  [15] in the fit.

Our fitting result for  $\theta$ , defined in Eq.(3), is  $|\theta| = 58.1^{+8.4}_{-7.3}$  degrees, which is consistent with  $|\theta| = 37^\circ$  and  $58^\circ$  recently determined also in  $\tau$  decays [21]. The predictions for branching ratios we get are summarized in Table 1 and Table 2. In case of the one multiplet, we take the values of resonance couplings from [10][11]. For the other cases, we use the fitting results presented in [15]. Comparison of the figures we have obtained for the  $\tau^- \rightarrow \omega \pi^- \nu_\tau$  spectral function and the invariant mass distributions for  $\omega K^-, \phi K^-$  between the experimental data are given in Fig.(3-5) respectively. Although different choices for  $\lambda_i$  affect the branching ratios, the invariant mass distributions are barely influenced. So we only plot the figures with  $\lambda' = 0.5, \lambda'' = 0, \lambda_0 = 0.125$ .

## REFERENCES

1. W.-M. Yao *et al.*(Particle Data Group), J. Phys. **G 33** (2006) 1.
2. K. W. Edwards *et al.*(CLEO Collaboration), Phys. Rev. **D 61** (2000) 072003.
3. K. Arms *et al.*(CLEO Collaboration), Phys. Rev. Lett **94** (2005) 241802.
4. K. Inami *et al.*(Belle Collaboration), Phys. Lett. **B 643** (2006) 5.
5. B. Aubert *et al.*(BABAR Collaboration), Phys. Rev. Lett **100** (2008) 011801.
6. G. Ecker *et al.*, Nucl. Phys. **B321** (1989)311; Phys. Lett. B **223** (1989) 425;
7. V. Cirigliano, *et al.*, Nucl. Phys. **B 753** (2006) 139.
8. B. Moussallam, Phys. Rev. **D 51** (1995) 4939.
9. M. Knecht and A. Nyffeler, Eur. Phys. J. **C 21** (2001) 659.
10. P. D. Ruiz-Femenia, A. Pich and J. Portolés, JHEP 07 (2003) 003.
11. V. Cirigliano, *et al.*, Phys. Lett. **B 596** (2004) 96.
12. M. Jamin, A. Pich and J. Portolés, Phys. Lett. **B 640** (2006) 176; Phys. Lett. **B 664** (2008) 78.
13. D. Gomez-Dumm, A. Pich and J. Portolés, Phys. Rev. **D 69** (2004) 073002.
14. P. Roig, AIP Conf. Proc. **964** (2007) 40.
15. Z.H. Guo, Phys. Rev. **D 78** (2008) 033004.
16. J. Gasser and H. Leutwyler, Annals Phys. **158** (1984) 142; Nucl. Phys. **B 250** (1985) 465.
17. V. Mateu and J. Portolés, Eur. Phys. J. **C 52** (2007) 325.
18. M. Suzuki, Phys. Rev. **D 47** (1993) 1252.
19. D. Gomez-Dumm, A. Pich and J. Portolés, Phys. Rev. **D 62** (2000) 054014.
20. I. Adachi *et al.*(Belle Collaboration), arXiv:0808.1059 (hep-ex).
21. H. Y. Cheng, Phys. Rev. **D 67** (2003) 094007.